Journal of Power Sources 199 (2012) 94–102

Contents lists available at SciVerse ScienceDirect

Journal of Power Sources

journal homepage: www.elsevier.com/locate/jpowsour

Deposition and activity stability of Pt–Co catalysts on carbon nanotube-based electrodes prepared by microwave-assisted synthesis

Chien-Te Hsieh*, Wei-Yu Chen, I-Ling Chen, Anup Kumar Roy

Department of Chemical Engineering and Materials Science, Yuan Ze Fuel Cell Center, Yuan Ze University, Taoyuan 32003, Taiwan

ARTICLE INFO

Article history:
Received 26 July 2011
Received in revised form 13 October 2011
Accepted 15 October 2011
Available online 20 October 2011

Keywords:
Pt–Co catalysts
Carbon nanotubes
Electrochemical activity
Microwave heating
Fuel cells

ABSTRACT

This work investigates the electrochemical activity and durability of bimetallic Pt–Co electrocatalysts on carbon nanotube (CNT) electrodes, which are prepared by using a microwave-assisted polyol process within a short period of ~6 min. Multilayered CNTs are directly grown on carbon paper (CP) substrate by catalytic chemical vapor deposition with Ni catalyzing the growth of CNTs. The as-grown CNTs are employed as the support for the subsequent Pt–Co catalysts, which are deposited on the CNTs by using one- and two-step microwave-assisted reduction processes. Physicochemical characterizations are conducted to identify particle dispersion, particle-size distribution, and Pt/Co atomic ratio in the binary catalysts. It has been shown that Pt–Co–CNT/CP electrocatalyst, prepared by two-step microwave heating (i.e., deposition of Pt, followed by Co addition), offers highly electrochemical surface area and stable activity during potential cycling (1000 cycles). Such Pt–Co crystallographic phases on CNT-based support are found to be more corrosion-resistant in acidic electrolyte and represent the preferred phase structure under the consideration of activity stability. The fact that the microwave-assisted deposition of Pt–Co catalysts promotes electrochemical activity and stability has a great advancement on the development of binary electrocatalysts for fuel-cell applications.

1. Introduction

Proton exchange membrane fuel cells (PEMFCs) and direct methanol fuel cells (DMFCs) possess high potentiality for use in electric power production and portable applications because of their high energy conversion efficiency and high power density [1–3]. One major concern to commercialise the fuel cells (including PEMFC and DMFC) is significantly related to its high cost. It is generally believed that gas diffusion layer and catalyst layer are crucial for the performance of membrane electrode assembly (MEA) in fuel cells. Platinum-based particles have been recognized as effective, though expensive, metallic electrocatalysts for oxygen reduction reaction and methanol oxidation in MEAs [4,5]. Traditionally, carbon-supported Pt particles are coated and dispersed on gas diffusion layers by simply using brushing, spray, screen-printing, or decal transfer [6]. However, there still remains one drawback of poor dispersion of Pt nanoparticles or Pt aggregation, resulting in a lower active surface area for efficient catalysis. Therefore, one way to resolve this problem is to deposit the Pt-based catalysts on three-phase reaction zones that allow effective gas and water diffusion, proton transport, and electron conduction in the catalyst sites.

Accordingly, activity improvement of electrochemical catalysts has an important role in determining the performance of MEAs. To improve this, two strategies have been proposed in this study: (i) design of gas diffusion electrodes and (ii) development of novel catalysts. Recently, pioneer studies have pointed out that the direct growth of multi-walled carbon nanotubes (CNTs) on carbon substrates (e.g., carbon cloth and carbon paper [CP]) and subsequently depositing Pt catalysts selectively on the CNTs lead to improvement in Pt utilization in PEMFCs [1,7–10]. Basically, CNTs consist of several coaxially arranged graphene sheets rolled into a cylinder that possesses a relatively high electrical conductivity [11,12]. Such Pt–CNT/CP configuration directs at: (i) facilitating the utilization efficiency; (ii) minimizing the Pt loading; and (iii) satisfying the requirements of gas accessibility, proton transport, and electronic continuity. In the other aspect, several Pt-based binary catalysts, such as Pt–Zn [3], Pt–Ru [13,14], Pt–Fe [15,16], Pt–Co [6,17–22], Pt–Ni [23,24], and Pt–Sn [25,26], with different atomic concentrations have been examined. In many cases, the catalytic activity of the bimetallic Pt-based catalysts has been demonstrated, showing that the activity is better than that of pure Pt. There are few reports, however, focused on CNT/CP as a support for the bimetallic Pt-based catalysts, which examined their electrochemical behavior [27].

* Corresponding author. Tel.: +886 3 4638800x2577; fax: +886 3 4559373.
E-mail address: cthsieh@saturn.yzu.edu.tw (C.-T. Hsieh).

0378-7753/$ – see front matter © 2011 Elsevier B.V. All rights reserved.
doi:10.1016/j.jpowsour.2011.10.055

Earlier attempts to deposit Pt catalysts on carbon substrates, such as CNTs and carbon powders, were conducted by chemical-wet approach using ethylene glycol as the reduction agent [20,28]. However, continuous efforts to develop alternative synthesis methods are required because this preparation technique based on chemical reduction cannot offer adequate control of particle size and shape. Our previous studies [14,16] also observed this phenomenon. Recently, several groups reported that microwave-assisted polyol method efficiently deposits Pt nanoparticles with great uniformity on CNTs [4,29] and carbon powders [30]. When compared with the traditional method, the microwave-assisted approach is found to be a better synthesis option with regard to its energy efficiency, speed, uniformity, and simplicity in execution. It is generally recognized that the pH value of the synthesis solution is the crucial factor in influencing catalyst particle size when using polyol reduction method [31]. High pH condition is capable of forming smaller particles due to the presence of ester stabilizer. Herein one efficient microwave-assisted process of preparing CNT/CP-supported bimetallic Pt–Co nanocatalysts is thus carried out in the Pt-containing solution at initial pH ~12. A comparison between one- and two-step microwave reductions has been made to characterize the electrochemical activity and durability of the as-prepared Pt–Co catalysts, based on the evaluation of electrochemically active surface area (S_{ESA}).

2. Experiment

2.1. Synthesis of Pt–Co–CNT/CP catalysts

The CNTs were directly grown on CP (TGPH-090, Toray) through a catalytic chemical vapor deposition (CCVD) process using wet-impregnated Ni as the catalyst for CNT growth. The procedure for the decoration of CNTs on CP substrate has been reported in our previous study [32,33]. The CP sample was made of fibers having a diameter of approximately 8–10 μm, and the surface of the carbon fiber was cleaned before deposition. The Ni catalyst layers were coated onto the CP surface by impregnating the CP in 1 M nickel nitrate at ambient temperature. The deposition of Ni on the side of CP served as the catalytic site for selective growth of CNTs. The growth process of CNTs was performed in a horizontal furnace at 850 °C for 1 h. The gaseous carbon precursor had a composition of $Ar:H_2:C_2H_2 = 94:1:5$ in v/v/v, precisely controlled by mass flow controllers. This synthesis technique enabled the growth of a large number of CNTs on the CP surface, giving a CNT/CP composite.

Pt–Co–CNT/CP catalysts were synthesized by microwave heating of ethylene glycol solutions of $PtCl_4$ and $Co(NO_3)_2{\cdot}6H_2O$ precursor salts. Prior to any treatment, CNT/CP composites were chemically oxidized by 1 M nitric acid at 85 °C for 1 h. Subsequently, the oxidized CNT/CP composites with an area of $5 \times 5\,cm^2$ were impregnated with a Pt-containing solution. A typical preparation consisted of the following compositions: 1 ml of 0.04 M $PtCl_4$, 1 ml of 0.24 M $Co(NO_3)_2$, and 1 ml of 0.04 M KOH. The weight ratio of Pt to Co was set at 36:64 in the ionic solution. They were mixed with 30 ml of ethylene glycol in a beaker. The pH value was around 11.7. The beaker was kept open and placed in the center of a household microwave oven and then under microwave power of 720 W. The deposition period for each step of microwave heating was set at 6 min. The metal-coated CNT/CP samples were then separated from the Pt ionic solution and subsequently dried in a vacuum oven at 105 °C overnight. To inspect the influence of deposition sequence on the activity of Pt–Co catalysts, three types of microwave heating were used to prepare different bimetallic catalysts: (i) simultaneous deposition of Pt and Co species; (ii) deposition of Pt followed by Co species; and (iii) deposition of Co followed by Pt species, which were designated as Pt–Co–m, Pt–Co, and Co–Pt, respectively.

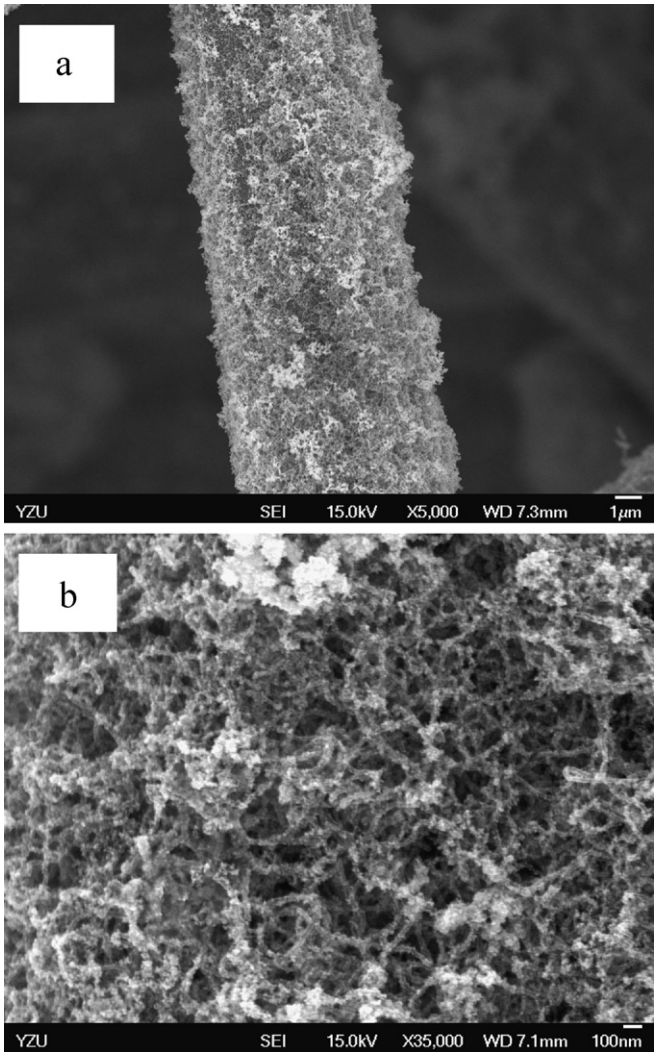

Fig. 1. FE-SEM micrographs of (a) CNTs grown by Ni catalyst layer on CP substrate and (b) Pt–Co catalysts deposited on CNT/CP composite.

2.2. Characterization of Pt–Co–CNT/CP catalysts

These binary catalyst samples, obtained from microwave-heated polyol synthesis, were characterized by using field-emission scanning electron microscopy (FE-SEM, JEOL JSM-5600) and high-resolution transmission electron microscopy (HR-TEM, JEOL, JEM-2100). The TEM study was carried out using a microscope operating at 200 kV. The CNT samples for the TEM analysis were prepared by ultrasonically dispersing the catalyst powders in ethanol. A drop of the suspension was applied onto a copper grid and was dried in the air. A thermogravimetric analyzer (TGA, Perkin–Elmer TA7) was used to analyze the amount of catalysts deposited on CNT/CP composites. The TGA analysis was conducted under an air atmosphere with a heating rate of 10 °C min^{-1} ramp between 30 °C and 1000 °C. The chemical composition of the catalysts was investigated by using X-ray photoelectron spectroscopy (XPS). The XP spectra were recorded with a Fison VG ESCA210 spectrometer and Mg Kα radiation.

2.3. Activity and durability measurements of Pt–Co–CNT/CP electrodes

Three types of CNT/CP composites decorated with Pt–Co nanoparticles were used to fabricate the electrodes for cyclic

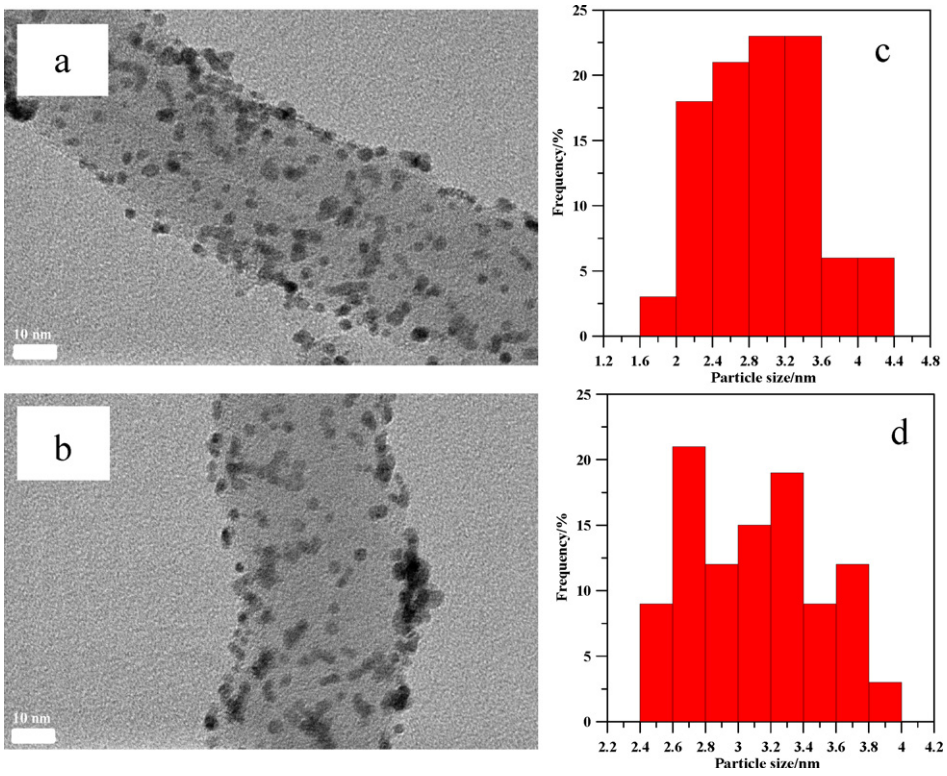

Fig. 2. HR-TEM micrographs of (a) Pt–Co–m and (b) Pt–Co catalysts. Particle size distributions of (c) Pt–Co–m and (d) Pt–Co catalysts.

voltammetry (CV) measurement. Electrochemical measurement of CNT-based electrodes was carried out at an ambient temperature using 1 M H_2SO_4 as the electrolyte solution. Pt wire and Ag/AgCl electrode served as the counter and reference electrodes, respectively. The working electrodes were constructed by pressing the CNT/CP composites onto the stainless steel foil that served as the current collector. CV measurements of the electrodes were performed in the potential range from −0.2 V to 0.8 V vs. Ag/AgCl. The potential scan rate and scan number were set at 50 mV s^{-1} and 1000 cycles, respectively, confirming

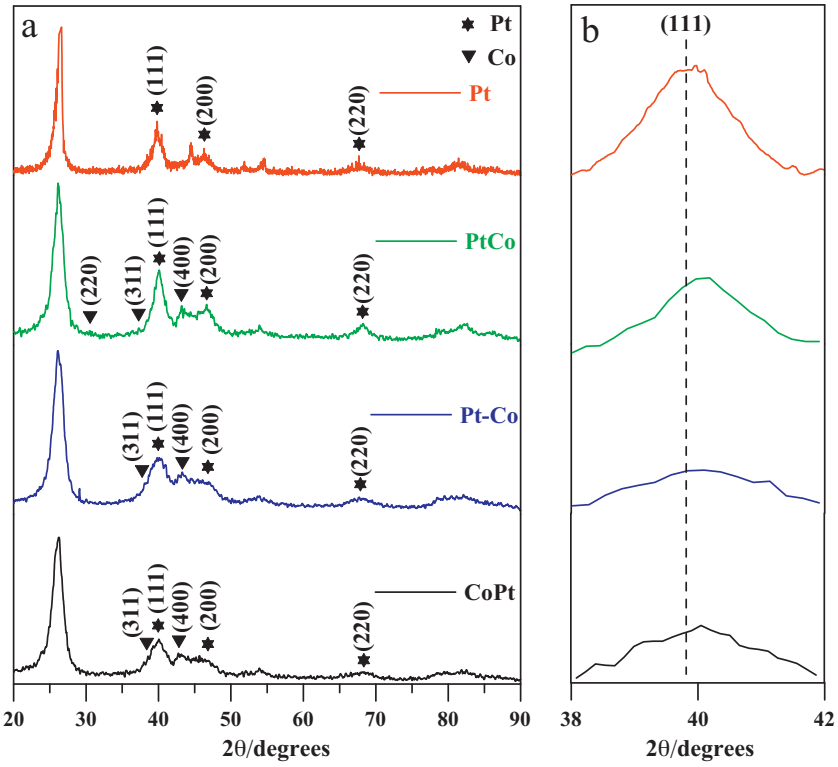

Fig. 3. (a) X-ray diffraction patterns of different types of Pt and Pt–Co samples supported at CNTs, and (b) Pt (1 1 1) for different types of Pt and Pt/Co samples.

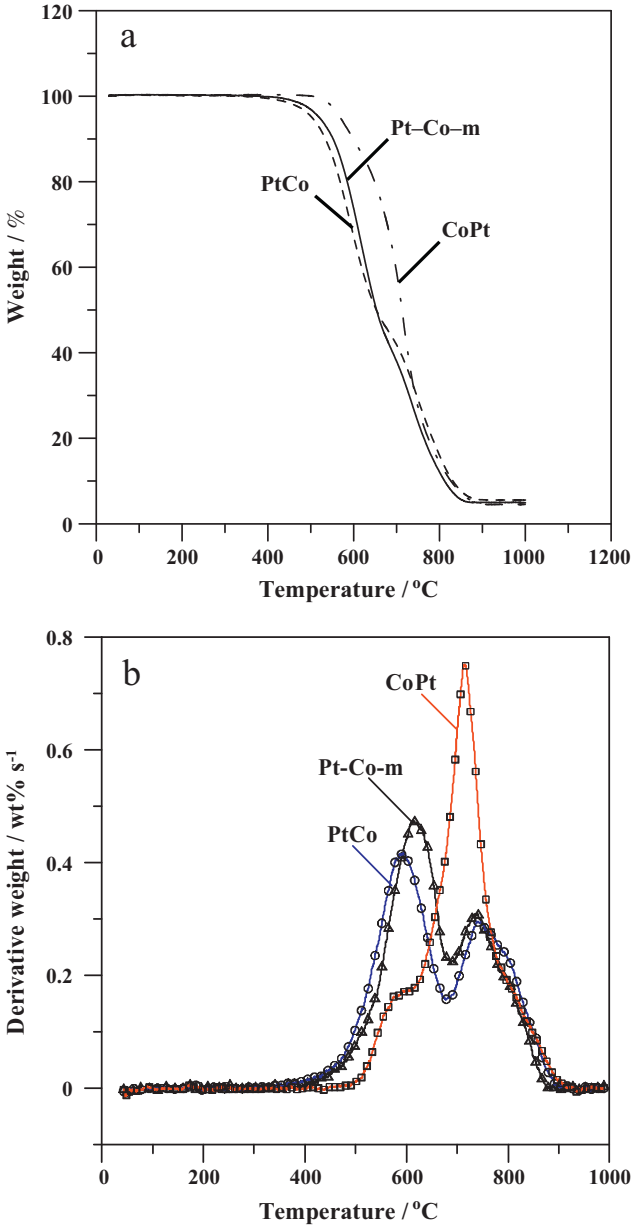

Fig. 4. TGA (a) weight-loss and (b) derivative-weight curves of different catalysts. The analysis was conducted under an oxygen atmosphere with a heating rate of 10 °C min^{-1} ramp between 30 °C and 1000 °C.

the activity and durability of bimetallic Pt–Co catalysts in acid electrolyte.

2.4. Performance of a single cell fabricated with Pt–Co electrodes

A single-cell test fixture was applied for evaluating the catalyst performance for an H_2/O_2-based fuel cell. The MEA, consisting of two Pt-based electrodes, was immersed in 5 wt% Nafion solution for 0.5 h. The MEA was thermally pressed (135 °C, 140 atm, 2 min) with a Nafion 212 membrane (DuPont Inc., USA) between the two electrodes. The MEA was then inserted between two graphite plates, which had a serpentine flow pattern. Two Teflon gaskets of 0.24 mm thickness were introduced between the membrane and the electrodes. Humidified hydrogen and oxygen gases were fed into the cell at a flow rate of 200 cm^3 min^{-1} and 400 cm^3 min^{-1}, respectively. The temperature of the single cell was maintained at

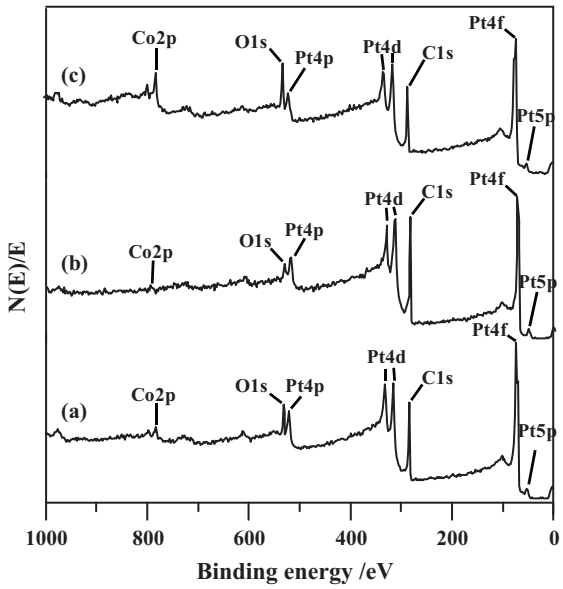

Fig. 5. Survey XPS spectra of different catalysts: (a) Pt–Co–m, (b) Pt–Co, and (c) Co–Pt.

60 °C, and the polarization curve and the power density of the cell were then characterized.

3. Results and discussion

3.1. Characterization of Pt–Co–CNT/CP composites

Fig. 1a presents the FE-SEM picture of the resulting CNT/CP after CCVD growth using Ni as the catalysts. It can be observed that a large number of CNTs cover the microscale carbon fiber. The as-grown CNTs are wavy with the lengths in the micrometer range and diameters in the range of 30–50 nm. The loading of CNTs over the CP substrates is approximately 0.8 mg cm^{-2}. Some bright particles on CNTs can be observed in Fig. 1b, which were identified as Pt–Co alloys by an electron diffraction X-ray spectroscopy. However, the dispersion degree of the catalysts cannot be clearly observed. This observation can be examined in Fig. 2a and b shows that the HR-TEM images of the resulting samples, Pt–Co–m and Pt–Co, respectively. The images clearly reflect that the small particles, attached to the outer surface of CNTs, have a uniform dispersion. However, the influence of the deposition sequence on the average size and uniformity seems to be minor. Fig. 2c and d shows the particle-size distributions of Pt–Co–m and Pt–Co, respectively. This statistical result was obtained from more than 100 Pt–Co nanoparticles, thus showing the distribution of the particle size. As it can be seen, both the bimetallic catalysts were homogeneously dispersed onto the surface of the CNTs, indicating a narrow particle-size distribution. The mean particle sizes were 3.2 and 3.1 nm for Pt–Co–m and Pt–Co, respectively.

The crystalline structure of Pt–Co catalyst was examined by XRD for each pair of the bimetallic nanoparticles deposited on the CNTs, as shown in Fig. 3a. It is generally believed that pure Pt has a face-centered cubic (fcc) structure. Peaks reveal at $2\theta \approx 40°$ and 47°, which can be characterized with the (1 1 1) and (2 0 0) planes, respectively [34], of the fcc structure of platinum. In addition, other diffraction peaks referred to cobalt metal emerged, confirming different pairs of Pt–Co catalysts on CNTs. After the addition of Co metal, the diffraction peaks of binary Pt–Co catalyst lead to broaden and shift to high 2θ values [35]. As shown in Fig. 3b, the 2θ of the (1 1 1) peak for Pt–Co catalyst higher than 40° shows a slight shift, when compared with the pure Pt at 39.9°. The formation of pure

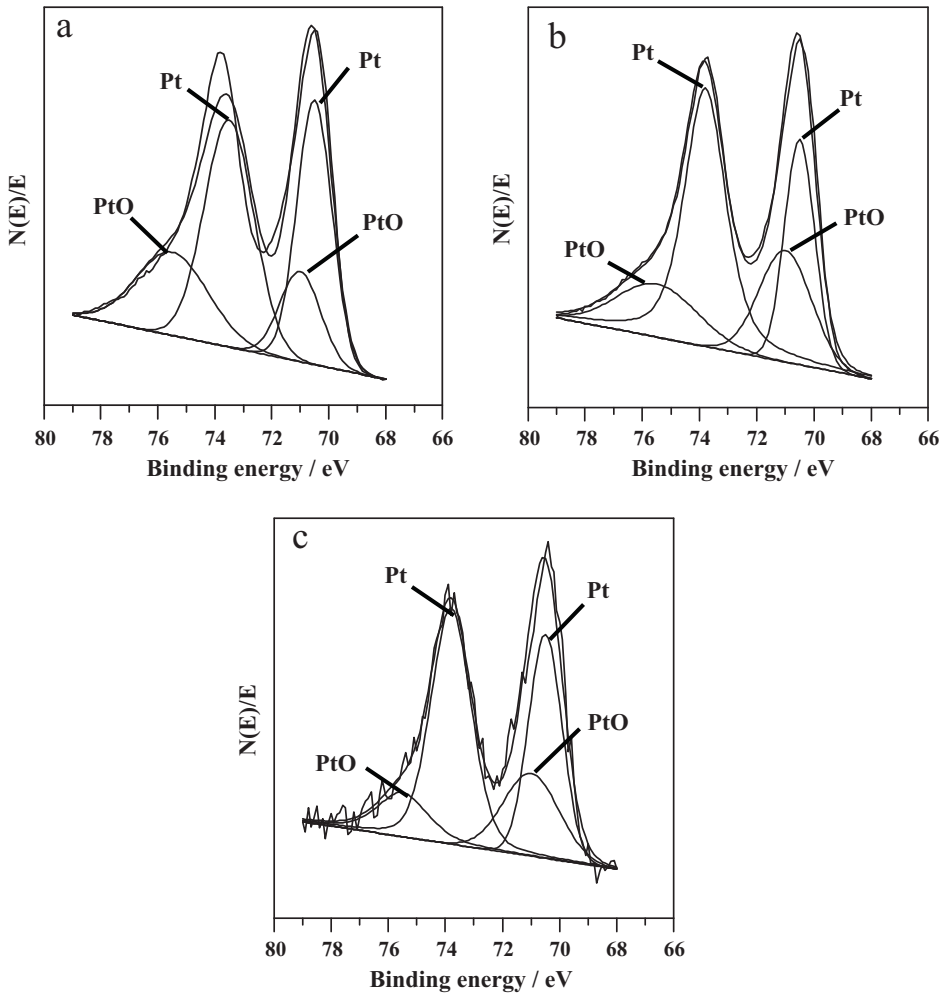

Fig. 6. XPS spectra of Pt 4f peaks for different catalysts: (a) Pt–Co–m, (b) Pt–Co, and (c) Co–Pt, deconvoluted by symmetric Gaussian functions.

Pt particles with *fcc* structure was confirmed, i.e., the lattice constant of 0.3910 nm agrees well with the crystallographic data [24]. The lattice constants of bimetallic catalysts are calculated to be 0.3900 nm (Pt–Co), 0.3882 nm (Pt–Co–m), and 90.3891 nm (Co–Pt), based on the diffraction peak in Fig. 3a. The introduction of cobalt atoms induces the deviation of lattice constant (0.24–0.72%), showing the partial intercalation of Co dopants into the *fcc* crystals. Previous studies also confirmed the change of lattice constant for Pt–Co catalysts, prepared by sputtering deposition [36] and reductive thermal annealing/alloying in solid state [37].

Fig. 4a and b depicts the three weight-loss and derivative-weight curves of the resulting catalysts respectively, showing a similar thermal stability and residual percentage on the CNT/CP composites. TGA analysis on these samples revealed that a major weight loss, corresponding to carbon gasification (i.e., amorphous carbon and multilayered CNTs), took place at 500–800 °C. This weight loss can be attributed to the fact that amorphous carbon (i.e., CP) has evolved and has a maximal gasification rate at around 500 °C, whereas the maximum gasification rate of multilayered CNT occurs at ca. 650 °C [38,39]. It is worth noting that all the samples have an identical residual weight percentage of ca. 5.0–5.2 wt%, which can be assigned to metallic Pt–Co catalysts. This finding implies that the deposition sequence in the microwave heating process does not alter the catalyst loading on CNT/CP composites. As shown in Fig. 4b, all bimetallic catalysts undergo a two-stage combustion stages but different temperature shifts, possibly originated from the atomic ratios of Pt to Co elements.

Basically, XPS is a powerful technique for analyzing surface compositions with detection depth of several nanometers. The survey scans for Pt–Co–m, Pt–Co, and Co–Pt samples are shown in Fig. 5. The spectra clearly indicate the presence of platinum, cobalt, carbon, and oxygen in the catalyst composites. The Pt 4f, Co 2p, C1 s, and O1 s peaks of the scan spectra have different binding energies of ca. 71.5, 778.5, 284.6, and 533.5 eV, respectively [40]. Quantitative analysis was carried out to estimate the surface Pt/Co atomic ratios, which showed the following results: Pt–Co–m (90:10), Pt–Co (96:4), and Co–Pt (83:17). It is interesting to note that the Pt/Co atomic ratios have different atomic concentrations in the prepared Pt–Co alloys. It can be inferred that the microwave-assisted synthesis tends to form Pt-rich catalysts, such as partial Pt–Co pair. This result implies that the Pt content contributes to a major proportion in the binary catalysts, leading to an atomic heterogeneity.

The Pt 4f peak consists of two pairs of doublets for three catalysts, as shown in Fig. 6a–c. It is known that Pt $4f_{5/2}$ exhibits a binding energy of 3.3 eV higher than Pt $4f_{7/2}$, that is, 74.8 eV (Pt $4f_{5/2}$) and 71.5 eV (Pt $4f_{7/2}$). Generally, the most intense doublet (i.e., 74.8 eV and 71.5 eV) can be assigned to metallic Pt (0), while the second set of doublets (i.e., 72.7 eV and 74.8 eV) corresponds to Pt (II) chemical state, such as PtO and $Pt(OH)_2$ [4,29,41,42]. It can be seen from these Pt 4f spectra that metallic Pt (0) plays as the major contributor over all Pt element contents (Pt [0] and Pt [II]). Moreover, the authors were unable to find any peak of Pt (IV), indicating the strong reduction from $PtCl_4$ to metallic Pt. This finding reflects that the microwave-assisted polyol method is capable of

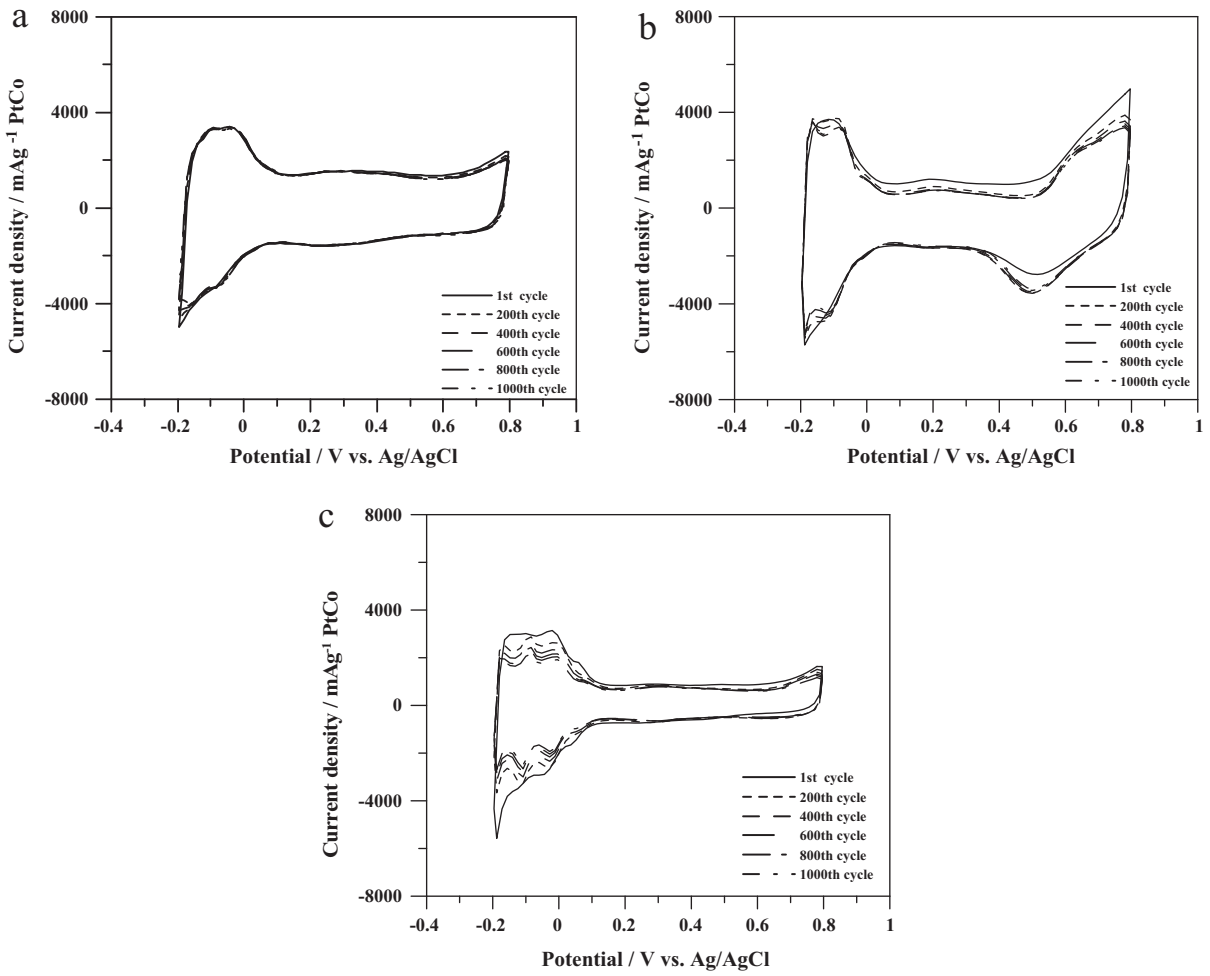

Fig. 7. Cyclic voltammograms of different electrodes: (a) Pt–Co–m, (b) Pt–Co, and (c) Co–Pt. Measurements were performed in 1 M H_2SO_4 at a sweep rate of 50 mV s^{-1} with potential cycling.

synthesizing metallic Pt content on the CNT surface. The ratios of Pt (0) to Pt (II) are found to have a slight change. This oxidation state of Pt can be presumably owing to one possible reason that oxygen chemisorption easily occurs and kinks at the surface sites of the Pt clusters.

3.2. Electrochemical behavior of Pt–Co–CNT/CP electrodes

The as-synthesized catalyst electrodes are characterized by CV (−0.2 V to 0.8 V vs. Ag/AgCl, 50 mV s^{-1}) in an electrolyte of 1 M H_2SO_4, and the resulting voltammograms within 1000 cycles are shown in Fig. 7. Basically, there are three regions exhibiting the CV feature: (i) adsorption–desorption of hydrogen (from −0.2 V to 0.2 V); (ii) double-layer formation (0.2–0.4 V); and (iii) oxide growth and stripping (0.4–0.8 V). This typical CV behavior confirms that CNT-supported Pt–Co binary catalysts, exhibiting electrochemical activity, can be successfully synthesized using the microwave heating with simplicity and short deposition period. The voltammetric features in the potential region from −0.2 V to 0.2 V represent the adsorption and desorption of a monolayer of hydrogen atoms on top of the Pt surface atoms [6,42]. The peaks for hydrogen and oxygen adsorption and desorption with the potential region from −0.2 V to 0.2 V vs. Ag/AgCl on the binary Pt–Co catalysts in H_2SO_4 are evidently shown. The presence of CNTs offers a catalyst support for dispersing bimetallic Pt catalysts with catalytic activity in the potential region of 0.2–0.4 V.

In comparison, there still remains a difference among the CV features owing to various surface atomic Pt/Co ratios, as shown in Fig. 7. The similar mean size of the as-grown Pt–Co catalysts reflects the fact that the surface atomic concentration plays a crucial role in affecting the electrochemical activity of the bimetallic nanocatalysts. It is worth noting that the oxide growth peak is essentially absent from the Pt–Co–m and Co–Pt catalysts, whereas it is more clearly defined for the Pt–Co case. The introduction of transition metals in the bimetallic catalyst reduces the required potential for water electrolysis and thus the associated carbon oxidation [43]. Similarly, the presence of Co-skin layer would promote the combined effect of water dissociation and Pt oxide growth and stripping.

Interestingly, the Pt–Co–CNT/CP electrode exhibits two evident peaks with good stability of 1000 cycles, namely, reversibility of adsorption-desorption of hydrogen and oxidation-reduction of Pt. This result strongly suggests that the design of Pt–Co catalyst can be applied to electrocatalysts for fuel-cell applications. To inspect this difference, the growth mechanism of binary Pt–Co catalysts should be taken into account as follows. In Pt–Co–CNT/CP, the Pt ions are initially adsorbed onto both the sidewalls and ends of the CNTs that possess oxygen functional groups (such as carboxyl, hydroxyl, and carbonyl groups) or dangling bonding. These oxygen groups and defects serve as adsorptive sites for adsorption of Pt ions in liquid phase, forming Pt intermediates. Microwave heating in ethylene glycol solution enables the reduction of Pt intermediates over the surface of CNTs, thus generating metallic Pt. The second step of

microwave-assisted synthesis selectively deposits and then dopes the Co species onto the Pt surface, inducing Pt–Co pair with high alloying. On the basis of the CV result, such Pt–Co crystallographic phases are found to be more corrosion-resistant in an acidic electrolyte and represent the preferred phase structure with regard to activity stability.

As shown in Fig. 7, the cathodic/anodic peak current of Co–Pt electrode gradually becomes weaker after cycling, reflecting a poor cycling ability. The Co species have first been deposited onto the CNT surface at the first-stage reduction. As Pt has larger molecular size than Co atoms, this would result in a complexity for the Pt insertion into the Co–Co pair. This can presumably be due to the low alloying degree or incomplete coverage of Pt skin on Co particle. It is well known that the dissolution of Co metals easily occurs in acid electrolyte [44]. Thus, this dissolution would result in a poor durability of Co-rich catalysts.

3.3. Durability of Pt–Co–CNT/CP electrodes

The CV features are used to estimate the electrochemical Pt surface areas of individual catalysts. The specific charge transfer, contributed from Pt–Co catalysts (Q_H), can be obtained from [45]:

$$Q_H = Q_T - Q_{CNT} \quad (1)$$

where Q_T is the total specific charge transfer in the hydrogen adsorption/desorption potential region, and Q_{CNT} is the double-layer capacitive charge transfer from the pure CNT electrode. The total charge transfer (Q_T) can be evaluated by integrating the CVs in the relevant potential region:

$$Q_T = \frac{1}{2\nu}\int_{-0.2}^{0.2} (I_d - I_a)\, dE \quad (2)$$

where ν is the sweep rate, I_d and I_a are the specific current of desorption and adsorption, respectively, and E is the potential. The S_{ESA} value, based on Q_H, can be determined by [43]:

$$S_{ESA} = \frac{Q_H}{210m} \quad (3)$$

where m is the catalyst loading in units of g cm^{-2}, and the factor 210, in units of μC cm^{-2}, is determined from electrical charge associated with monolayer adsorption of hydrogen on Pt.

Basically, the durability of Pt–Co electrocatalysts can be investigated by using the variation of S_{ESA} values with potential cycling. On the basis of the results shown in Fig. 7, the values of S_{ESA} for each cycle were evaluated, and the results are presented in Fig. 8a. At the initial stage of potential cycling, Co–Pt exhibited the highest activity among these catalysts. Both the S_{ESA} values of Pt–Co–m and Pt–Co were found to have a stable activity within 1000 cycles, whereas the S_{ESA} value of Co–Pt clearly showed a sharp decay during potential cycling. Almost 40% decay clearly revealed the deactivation of Co–Pt electrode, that is, ca. 30.2 m^2 g^{-1} Pt at 1000th cycle. Again, this can be attributed to one possible reason of the dissolution of metallic cobalt in acidic electrolyte, forming cationic Co species, which is likely to increase the separation of Pt from CNT support. Among these catalysts, Pt–Co catalyst exhibits the highest S_{ESA} value of 40.3 m^2 g^{-1} after potential cycling. This S_{ESA} value shows the same order of magnitude compared with Pt–Co catalysts by other fabrication routes, such as electroless deposition (Pt–Co catalysts on carbon black, S_{ESA}: 32.0 m^2 g^{-1}) [46], microemulsion technique (Pt–Co catalyst on carbon black, S_{ESA}: 33.9 m^2 g^{-1}) [47], electrodeposition method ($Pt_{10000}Co$ on Ti foil substrate, S_{ESA}: 115 m^2 g^{-1}) [48], and liquid metal precursor impregnation method ($Pt–Co_3$ on glassy carbon, S_{ESA}: 36–45 m^2 g^{-1}) [49].

To clarify the durability, the other version of normalized S_{ESA} varied with CV cycle number, as shown in Fig. 8b. The variations

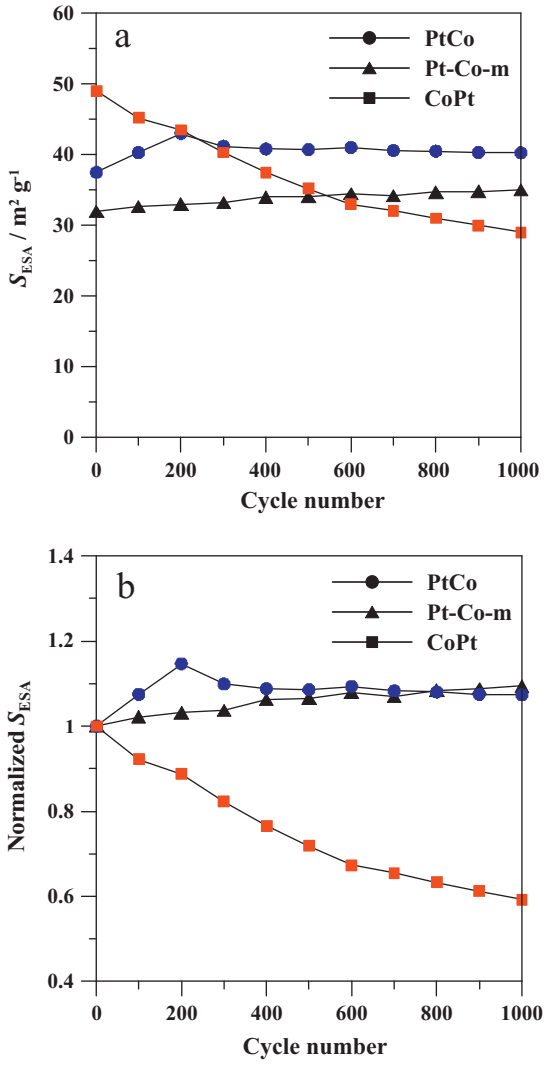

Fig. 8. (a) The S_{ESA} and (b) the normalized S_{ESA} value as a function of cycle number for different electrodes.

clearly show that both Pt–Co and Pt–Co–m catalysts offer higher electrochemical stability, compared with Co–Pt catalyst. It is generally recognized that the degradation of S_{ESA} originates from the dissolution and agglomeration of Pt nanoparticles. This finding was also observed elsewhere [50]. Accordingly, the analysis of relative activity demonstrates that the deposition sequence of microwave-assisted synthesis acts a key role in affecting not only catalytic activity but also electrochemical stability.

Generally, three possible mechanisms affecting the loss of S_{ESA} are proposed: (i) Pt migration on carbon support; (ii) Pt growth through Ostwarld ripening; and (iii) unsupported Pt particle owing to corrosion of carbon support [5]. After 1000 cycles, the final values of S_{ESA} exhibited the following order: Pt–Co (43.5 m^2 g^{-1}) > Pt–Co–m (33.4 m^2 g^{-1}) > Co–Pt (30.2 m^2 g^{-1}). The potential cycling test confirmed that both the electrochemical activity and the cycling stability of Pt–Co electrode are significantly improved. This finding revealed one vital factor in promoting the activity and durability of binary Pt–Co catalysts: deposition sequence. Incorporation of the above-mentioned key factors could result in well-mixed binary Pt–Co alloys, thus demonstrating long-term durability in an acidic electrolyte. Such a combination of Pt–Co cluster could serve as a potential candidate to replace pure Pt catalyst for fuel-cell applications.

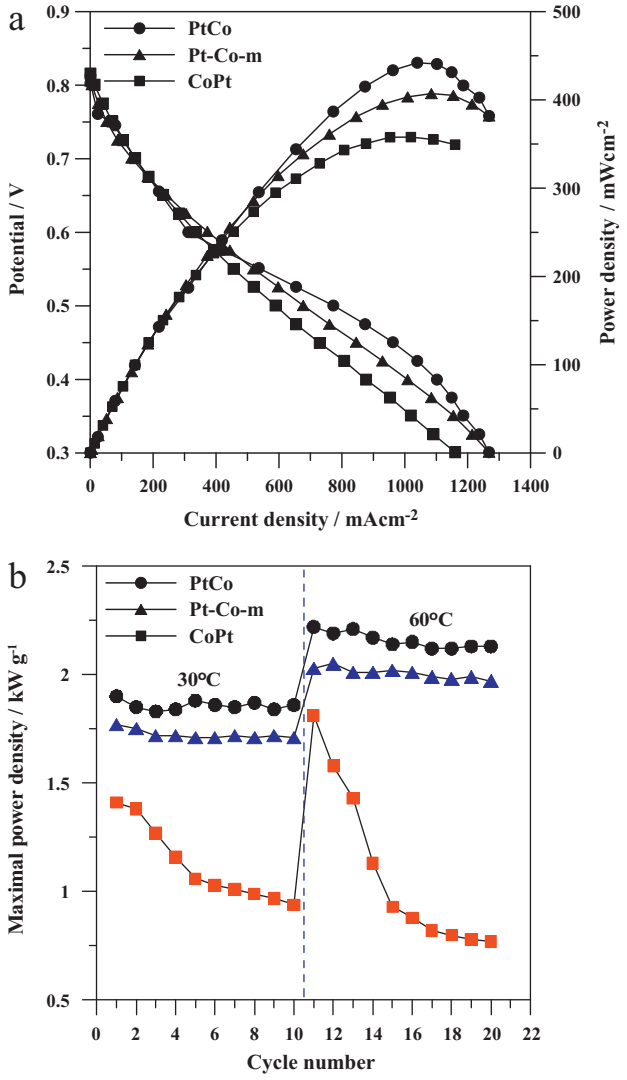

Fig. 9. (a) Polarization curves of single cells, fabricated with different catalyst electrodes, under H_2/O_2 flows at 60 °C. (b) The variation of maximal power density of PEMFC with cycle number at 30 and 60 °C.

To approach the practical application, the polarization curves of a single cell, fabricated with different Pt–Co electrodes, at 60 °C with H_2/O_2 are shown in Fig. 9. The Pt–Co loadings on the catalyst electrodes are set at ~0.20 mg cm^{-2}. The cell performance for each catalyst is quite similar up to 0.6 V, after which there is some separation of performance. This difference can be attributed to the fact that these MEAs equipped with Pt–Co electrodes exhibit different catalytic activity in hydrogen oxidation and oxygen reduction reactions. The curves also confirm that the Pt–Co cell displays a maximal power density of 442 mW cm^{-2}, higher than Pt–Co–m (407 mW cm^{-2}) and Co–Pt (357 mW cm^{-2}) cells. The maximal power density based on the Pt–Co loading has an order as follows: Pt–Co (2.21 kW g^{-1}) > Pt–Co–m (2.04 kW g^{-1}) > Co–Pt (1.79 kW g^{-1}). The maximal power density for MEA fabricated with Pt-deposited CNT electrodes has been reported [27]. For comparison, the power density of Pt–Co catalyst is higher than that of the Pt catalyst electrode, i.e., 2.21 kW g^{-1} > 2.06 kW g^{-1}. The enhanced power density reflects that the design of binary Pt–Co catalyst prepared by rapid microwave heating is effective in fuel-cell applications, showing the feasibility for the replacement of pure Pt catalyst electrodes.

To examine the stability of Pt–Co catalyst electrodes, the cycling performance of MEAs in the PEMFC at different temperatures was investigated. The plot of maximal power density of PEMFC versus cycle number is illustrated in Fig. 9b. This correlation clearly evidences that both Pt–Co and Pt–Co–m catalyst electrodes keep the power efficiency within the temperature window after cycling, while Co–Pt catalyst shows a significant decay of power efficiency. It should be noted that the Co–Pt catalyst electrode operated at 60 °C significantly reduce the cell performance, resulting in a poor durability. This can be ascribed to the fact that the higher operating temperature dramatically speeds up the dissolution and separation of Co–Pt nanoparticles from the surface of CNTs. Among these electrodes, the Pt–Co catalyst exhibits the best durability, resulting from a strong adhesion between CNTs and bimetallic Pt-based catalysts and an excellent catalytic activity in MEA after cycling at 30 and 60 °C. On the basis of the results, this confirms the Pt–Co catalyst, prepared by the efficient microwave heating, can serve as the potential candidate for replacing pure Pt catalyst.

4. Conclusions

In this study, the use of microwave-assisted polyol reduction as the deposition technique for preparing binary Pt–Co alloys was investigated as a way to reduce the cost through an enhanced activity with excellent durability. A large amount of CNTs were selectively grown on the CP substrate by CCVD with wet-impregnated Ni catalyzing the growth of CNTs. The as-grown CNTs were employed as the support for the subsequent Pt–Co catalysts, which were deposited onto the CNTs by one- and two-step microwave heating. Furthermore, HR-TEM characterization was conducted to identify the little influence of deposition cycling on the alloy size, but well dispersion of Pt–Co catalysts onto the oxidized CNTs. XPS analysis confirmed that the microwave heating enabled the formation of metallic Pt and different Pt/Co atomic ratios in the binary catalysts. The analysis further revealed that Pt–Co electrocatalyst, prepared by two-step microwave heating, could exhibit higher S_{ESA} value and excellent durability during the potential cycling (1000 cycles), when compared with the other two catalysts. Such Pt–Co crystallographic phases on CNT-based support are found to be more corrosion-resistant in acidic electrolyte and represent the preferred phase structure with regard to activity stability.

Acknowledgements

The authors are very grateful for the financial support from the National Science Council of the Republic of China under the contracts NSC 100-2120-M-155-001 and NSC 100-2221-E-155-031.

References

[1] C. Wang, M. Waje, X. Wang, J.M. Tang, R.C. Haddon, Y. Yan, Nano Lett. 4 (2003) 345.
[2] J.H. Wee, K.Y. Lee, S.H. Kim, J. Power Sources 165 (2007) 667.
[3] A. Miura, H. Wang, B.M. Leonard, H.D. Abruna, F. DiSalvo, J. Chem. Mater. 21 (2009) 2661.
[4] D.M. Han, Z.P. Guo, R. Zeng, C.J. Kim, Y.Z. Meng, H.K. Liu, Int. J. Hydrogen Energy 34 (2009) 2426.
[5] S. Takenaka, H. Matsumori, H. Matsune, H. Matsune, E. Tanabe, M.J. Kishida, Electrochem. Soc. 155 (2008) B929.
[6] S. Koh, J. Leisch, M.F. Toney, P. Strasser, J. Phys. Chem. C 111 (2007) 3744.
[7] A.M. Kannan, P. Kanagala, V. Veedu, J. Power Sources 192 (2009) 297.
[8] V. Kamavaram, V. Veedu, A.M. Kannan, J. Power Sources 188 (2009) 51.
[9] C.H. Wang, H.Y. Du, Y.T. Tsai, C.P. Chen, C.J. Huang, L.C. Chen, K.H. Chen, H.C. Shih, J. Power Sources 171 (2007) 55.
[10] M. Lebert, M. Kaempgen, M. Soehn, T. Wirth, S. Roth, N. Nicoloso, Catal. Today 143 (2009) 64.
[11] P.H. Maheshwari, R.B. Mathur, Electrochim. Acta 54 (2009) 7476.
[12] Z. Tang, C.K. Poh, Z. Tian, J. Lin, H.Y. Ng, D.H.C. Chua, Electrochim. Acta 56 (2011) 4327.

[13] L. Li, Y. Xing, Phys. J. Chem. C 111 (2007) 2803.
[14] C.T. Hsieh, Y.W. Chou, W.Y. Chen, J. Alloys Compd. 466 (2008) 233.
[15] W. Chen, J. Kim, S. Sun, S. Chen, Langmuir 23 (2007) 11303.
[16] C.T. Hsieh, J.Y. Lin, J.L. Wei, Int. J. Hydrogen Energy 34 (2009) 685.
[17] P. Paunovic, I. Radev, A.V. Dimitrov, O. Popovski, E. Lefterova, E. Slavcheva, S.H. Jordanov, Int. J. Hydrogen Energy 34 (2009) 2866.
[18] E.I. Santiago, L.C. Varanda, H.M. Villulas, J. Phys. Chem. C 111 (2007) 3146.
[19] Y. Xu, A.V. Ruban, M. Mavrikakis, J. Am. Chem. Soc. 126 (2004) 4717.
[20] J.R.C. Salgado, E. Antolini, E.R. Gonzalez, J. Phys. Chem. B 108 (2004) 17767.
[21] C.T. Hsieh, J.L. Wei, J.Y. Lin, W.Y. Chen, J. Power Sources 183 (2008) 91.
[22] T. Lopes, E. Antolini, F. Colmati, E.R. Gonzalez, J. Power Sources 164 (2007) 111.
[23] C.H. Yen, K. Shimizu, Y.Y. Lin, F. Bailey, I.F. Cheng, C.M. Wai, Energy Fuels 21 (2007) 2268.
[24] H. Yano, M. Kataoka, H. Yamashita, H. Uchida, M. Watanabe, Langmuir 23 (2007) 6438.
[25] D. Lee, S. Hwang, I. Lee, J. Power Sources 145 (2005) 147.
[26] C. Dupont, Y. Jugnet, D. Loffreda, J. Am. Chem. Soc. 128 (2006) 9129.
[27] C.T. Hsieh, W.M. Hung, W.Y. Chen, J.Y. Lin, Int. J. Hydrogen Energy 36 (2011) 2765.
[28] S.C. Zignani, E. Antolini, E.R. Gonzalez, J. Power sources 182 (2008) 83.
[29] W. Chen, J. Zhao, J.Y. Lee, Z. Liu, Mater. Chem. Phys. 91 (2005) 124.
[30] Z. Liu, X.Y. Ling, X. Su, J.Y. Lee, J. Phys. Chem. B 108 (2004) 8234.
[31] C. Bock, C. Paquet, M. Couillard, G.A. Botton, B.R. MacDougall, J. Am. Chem. Soc. 126 (2004) 8028.
[32] C.T. Hsieh, W.Y. Chen, F.L. Wu, Carbon 116 (2008) 677.
[33] C.T. Hsieh, W.Y. Chen, Carbon 48 (2010) 612.
[34] E.S. Steigerwalt, G.A. Deluga, C.M. Lukehart, J. Phys. Chem. B 106 (2002) 60.
[35] J. Prabhuram, T.S. Zhao, Z.X. Liang, R. Chen, Electrochim. Acta 52 (2007) 2649.
[36] A. Bonakdarpour, K. Lake, K. Stevens, J.R. Dahn, J. Electrochem. Soc. 155 (2008) B108.
[37] S. Koh, C. Yu, P. Mani, R. Srivastava, P. Strasser, J. Power Sources 172 (2007) 50.
[38] M. Corrias, B. Caussat, A. Ayral, J. Durand, Y. Kihn, Ph. Kalck, Ph. Serp, Chem. Eng. Sci. 58 (2003) 4475.
[39] C.T. Hsieh, J.Y. Lin, Powder Technol. 192 (2009) 16.
[40] C.D. Wagner, W.M. Riggs, L.E. Davis, J.F. Moulder, G.F. Muilenberg, Handbook of X-ray Photoelectron Spectroscopy, Perkin–Elmer Co, Minnesota, 1979.
[41] A. Halder, S. Sharma, M.S. Hegde, N. Ravishankar, J. Phys. Chem. C 113 (2009) 1466.
[42] Y. Xing, J. Phys. Chem. B 108 (2004) 19255.
[43] Y. Shao, G. Yin, Y. Gao, P. Shi, J. Electrochem. Soc. 153 (2006) A1093.
[44] M. Pourbaix, Atlas of Electrochemical Equilibria in Aqueous Solutions, Pergamon Press, Oxford, 1966.
[45] C.T. Hsieh, Y.W. Chou, J.Y. Lin, Int. J. Hydrogen Energy 32 (2007) 3457.
[46] N. Travitsky, T. Ripenbein, D. Golodnitsky, Y. Rosenberg, L. Burshtein, E. Peled, J. Power Sources 161 (2006) 782.
[47] P. Hernández-Fernández, S. Rojas, P. Ocón, J.L. Gómez de la Fuente, P. Terreros, M.A. Peña, J.L. García-Fierro, Appl. Catal. B Environ. 77 (2007) 19.
[48] C. Xu, Y. Su, L. Tan, Z. Liu, J. Zhang, S. Chen, S.P. Jiang, Electrochim. Acta 54 (2009) 6322.
[49] M. Oezaslan, P. Strasser, J. Power Sources 196 (2011) 5240.
[50] Y. Chen, J. Wang, H. Liu, R. Li, X. Sun, S. Ye, S. Knights, Electrochem. Commun. 11 (2009) 2071.